A1608

Optimizing GDC electrolytes of FESCs: Insights into microstructure formation and cell processing

Denise Ramler (1,2), Luzie Wehner (3), Christian Lenser (1), Olivier Guillon (1,2), Norbert H. Menzler (1,2)
(1) Institute of Energy and Climate Research (IEK), Materials Synthesis and Processing (IEK-1), Forschungszentrum Jülich GmbH 52425 Jülich/Germany;
(2) Institute of Mineral Engineering, RWTH Aachen University (GHI), 52074 Aachen/Germany;
(3) Institute of Energy and Climate Research (IEK), Structure and Function of Materials (IEK-2), Forschungszentrum Jülich GmbH 52425 Jülich/Germany;
Tel.: +49-2461 61-4596
d.ramler@fz-juelich.de

Abstract

Gadolinium doped ceria (GDC) is regarded as a promising alternative to 8YSZ in SOC applications due to its improved ionic conductivity and mixed ionic-electronic conductivity offering potential benefits as fuel electrode material. However, interdiffusion at the active interface between YSZ electrolyte and Ni-GDC electrode results in structural and performance degradation. Thus, implementation of a GDC electrolyte with a Ni-GDC electrode should enhance cell performance, as no interdiffusion zones are formed at the active interface.
The incorporation of GDC into a fuel electrode-supported cell poses several challenges. Especially, the appropriate microstructure formation of the electrolyte during the co-sintering of multiple layers requires a fundamental understanding of each processing step. For this reason, cell production, entirely based on screen printing, was systematically investigated with focus on a three-layer GDC/YSZ/GDC electrolyte that can be sintered on a Ni-GDC fuel electrode.
Investigations have shown that a pre-treatment of the starting powder can significantly alter the sintered electrolyte structure. Therefore, the influence of powder treatment at various temperatures and the addition of dopants on the sintering behavior was investigated. The powders were characterized by their particle size distribution (PSD), measurements of the specific surface area (SSA) via BET, scanning electron microscopy (SEM) and their sintering behavior via dilatometry measurements. Utilizing rheological measurements, new screen-printing pastes were formulated and optimized regarding their flow behavior. Dispersion stability for non-polar solvents, linear viscoelastic behavior (LVE) and time-dependent structural changes within the pastes after deposition (thixotropy) were evaluated and adjusted. Ultimately, half and full cells were produced. Cell bending after co-sintering of the electrolyte was quantified using white light topography and minimized by adjusting layer thicknesses in the composite. Cross-sections indicate appropriate layer microstructures while performance testing of these three-layer electrolyte cells is currently ongoing.

Introduction

Fuel gas electrodes based on doped CeO_2 (e.g. gadolinium doped ceria (GDC)) are the state-of-the-art in electrolyte-supported cells (ESCs) and metal-supported cells (MSCs). However, the cost-efficient integration of this material in high-performance fuel-electrode supported cells (FESCs) has not yet been fully established. A prototype developed at Forschungszentrum Jülich as a novel, high-performance FESC with a GDC electrolyte and a Ni-GDC fuel electrode, shows very good performance compared to state-of-the-art FESCs [1]. Despite the overall good performance, at high current densities in electrolysis mode, these cells failed due to cracks appearing in the electrolyte caused by mechanical stresses in the multi-layer system [2]. The aim is therefore to improve the microstructure of the layer composite in order to achieve not only an increase in performance but also an increase in mechanical integrity. Additionally, the two barrier layers inside the 3-layer electrolyte were formerly produced via sputtering. These shall now also be replaced by screen-printed layers to streamline the process and further reduce costs.
However, achieving dense electrolyte layers with good adhesion using suspension-based processes is challenging and requires a thorough understanding of both the manufacturing and the co-sintering processes. Usually, screen-printed GDC layers exhibit high residual porosities [3]. Therefore, with the help of investigations of the sintering behavior of GDC, as well as a comprehensive analysis of the relevant rheological properties of screen-printing pastes, an attempt was made to decipher the essential influencing factors in the production of dense GDC electrolyte layers.

1. Scientific Approach

One reason for the high residual porosity in sintered screen-printed GDC layers could be a mismatched sintering behavior of the material to the yttria-stabilized-zirconia (YSZ) electron-blocking layer and especially the NiO-YSZ substrate. For YSZ based solid oxide cells, studies have shown that an adaptation of the sintering behavior of YSZ to the NiO-YSZ substrate by pre-calcining and grinding the powder could lead to an increased density as well as to a minimization of cell bending during sintering [4]. Therefore, when introducing a GDC layer into this multilayer composite, an adjustment of the sintering behavior of the GDC is also likely to be advantageous for densification.
Furthermore, a low sintering activity of the GDC at the relevant temperatures can hinder the densification of the layer [5]. Further studies have shown that the poor densification behavior of GDC can be improved by the addition of different cations due to increase oxygen mobility. This, however, was also shown to lead to a decrease of the sinter-onset temperature, posing a possible difficulty for aligning sinter behaviors of multiple materials [6]. Therefore, a careful investigation of the influence of pre-calcination temperature and the doping of cations is necessary to minimize the porosity within the GDC layer.

Another key aspect in the production of high-quality and dense screen-printed layers is optimizing the fabrication method. In screen-printing, understanding and adjusting the rheological properties of the ceramic pastes or inks is vital for obtaining desired microstructures. Studies suggest that establishing a link between the ink composition and its rheology greatly benefits the optimization process as it provides fundamental information about the influence of paste rheology on the resulting sintered microstructure and how it can be properly adjusted [7]. The main rheological properties of screen-printing pastes for SOC applications are pseudoplasticity, viscoelasticity and thixotropy, with the later two gaining more attention over the past few years. One method of characterizing viscoelasticity and thixotropy is utilizing more advanced oscillatory rheometry [8, 9]. The

measured response from such an oscillation experiment can be divided into an elastic and viscous component individually, thus providing access to the quantitative determination of the elastic and viscous properties of a material. Energy that is stored within a paste upon excitation is represented by the storage modulus G' and corresponds to elastic behavior. On the other hand, energy that dissipates is expressed with the loss modulus G'', which describes viscous behavior.
Two points of interest while analyzing the viscoelasticity of pastes are the size of the linear viscoelastic region (LVR), that determines a load range in which the viscoelasticity of a material is independent of strain or stress, and the transition into yielding and start of flow. This yield point indicates a load that must be induced during the paste application process for successful printing and marks the end of the LVR. A recently introduced and more practical approach to describing the viscoelastic yielding behavior is by employing the flow transition index (FTI). It is the ratio of the flow point σ_f (G' = G'') to the more traditional definition of the yield point σ_y, where G' starts to deviate from linearity [10]:

$$FTI = \frac{\sigma_f}{\sigma_y} \quad (1)$$

This allows for a distinction between abrupt yielding (FTI close to 1), indicating a brittle material, and the more gradual yielding of a flexible material (FTI >> 1). Information about the yielding behavior might be helpful in adjusting printer settings (e.g., squeegee speed, screen mesh size) for achieving complete and even prints.
Regarding the leveling of pastes, the most practical approach is to characterize the thixotropy behavior by measuring the recovery times using the 3-interval-thixotropy-test (3ITT). Usually, the end of recovery is indicated in such a test by the intersection point of storage and loss modulus in the 3rd interval, after which G' > G'' applies [10].

2. Experiments

Multiple batches of the as-received $Gd_{0.1}Ce_{0.9}O_{1.95}$ powder (GDC10-M, Fuelcellmaterials, USA) were calcined at either 1130 °C, 1230 °C or 1340 °C for 3 h. The YSZ powder used in the YSZ barrier layer (TZ-8Y Zirconia, Tosoh, Japan) was also calcined at 1230 °C for 3 h. All powders were subsequently milled using either a tumbling mixer (Turbula T2F, Willy A. Bachofen AG, Switzerland) or a planetary micro mill (Pulverisette 7 premium line, FRITSCH GmbH, Germany) resulting in bimodal and unimodal particle size distributions (PSD), respectively. A fraction of the GDC powder calcined at 1230 °C with a bimodal PSD after milling was then additionally doped with cobalt ions. For this, the powder was dispersed in deionized water using a magnetic stirrer. Upon complete homogenization of the dispersion, 0.25 g of cobalt(II) nitrate hexahydrate ($Co(NO_3)_2$ 6 H_2O, Alfa Aesar) were added to the suspension. Under continuous stirring, the mixture was heated to 120 °C for several hours, until the suspension decomposed to a highly viscous slurry. This slurry was then completely dried at 120 °C. The resulting powder was ground in a mortar before calcination at 400 °C for 2 h to transform the nitrates into oxides. This should result in non-uniform coating of CoO on the GDC particles. During sintering, this would then transform into a solid solution of 0.5 mol % of CoO inside the GDC (gadolinium cobalt doped cerium oxide GCDC).
All powders were characterized for their particle size distributions via laser scattering (LA-950, HORIBA Europe GmbH, Germany) and for their specific surface area (SSA) by nitrogen adsorption (Area Meter II, Juwe Laborgeräte GmbH, Germany).

To investigate the sintering behavior of these powders, 8 mm uni-axially pressed pellets were prepared. Dilatometric isothermal holding measurements were carried out using a NETZSCH DIL 402 Expedis Classic dilatometer. The samples were heated up to 1400 °C with a ramp of 3 K/min. After holding this temperature for 5 h, the samples were cooled down again with a rate of 5 K/min, which is analogous to the co-sintering program used for the SOC half cells.

In order to investigate the relationship between the microstructure development of screen-printed electrolyte layers and rheological properties, a total of 7 pastes were produced from these powders. In addition to the ceramic powder, the main components of the pastes are terpineol as a solvent, a dispersant (KD2, Croda International Plc, United Kingdom) and ethyl cellulose with different chain lengths as a binder. The pastes were homogenized using a 3-roll mill (80E, EXAKT Advanced Technologies GmbH, Germany). The formulation of the pastes was selected in such a way that conclusions about the effect of particle size distribution, binder type and binder content can be drawn. An overview of the pastes is found in Table 1.

Table 1: Listing of all investigated pastes. Information about the particle size distribution of each powder is given as well as the calcination temperature. The binder content is given in wt.%. The binder type is presented as either 45 cp ethyl cellulose (EC) or 10 cp ethyl cellulose.

Paste	Powder	PSD	d_{10} / d_{50} / d_{90} (µm)	Binder
A	GDC1130	bimodal	0.07 / 0.10 / 0.27	3 % 45 cp EC
B	GDC1230	bimodal	0.07 / 0.11 / 0.27	3 % 45 cp EC
C	GDC1230	bimodal	0.07 / 0.11 / 0.27	4 % 45 cp EC
D	GDC1340	bimodal	0.06 / 0.10 / 0.76	3 % 45 cp EC
E	GDC1230	unimodal	0.07 / 0.10 / 0.16	3 % 45 cp EC
F	GDC1230	unimodal	0.07 / 0.10 / 0.16	3 % 10 cp EC
G	GCDC1230	bimodal	0.07 / 0.11 / 0.27	3 % 45 cp EC

The rheological measurements were carried out using the modular compound rheometer Physica MCR 301 (Anton Paar Germany GmbH, Germany). The data was collected using serrated parallel plates with a plate diameter of 25 mm and a plate spacing of 0.5 mm. Each measurement was performed at 20 °C and maintained via a temperature control unit (Julabo F25-EH, JULABO GmbH, Germany). To obtain the viscoelastic properties of the pastes, oscillatory amplitude sweep tests were conducted in a strain range γ of 0.1 – 1000 % with an angular frequency ω of 10 rad/s. For the evaluation of the thixotropic behavior, rest conditions for the first interval of the 3ITT were set to be at a strain γ of 1 %, which was held constant for 60 s. To simulate the printing process in the second interval, the pastes were subjected to very high shear rates of 3000 s^{-1} for 5 s in rotational mode. Quasi-undisturbed structure rebuilding of the paste was then analyzed in the 3rd interval using the same conditions as in the 1st interval.

Finally, half cells were prepared by printing NiO-GDC fuel electrodes on tape-cast NiO-YSZ substrates, followed by printing the 3-layer electrolyte using a semi-automatic screen printer (EKRA E-2, ASYS Group, Germany). A complete depiction of the manufacturing process is provided in Fig. 1. The resulting microstructures were analysed using a confocal laser microscope (Keyence Color 3D laser scanning microscope VK-9710, Keyence

Corporation, Japan) and scanning electron microscopy (SEM) (TM3000, Hitachi High-Technologies Corporation, Japan).

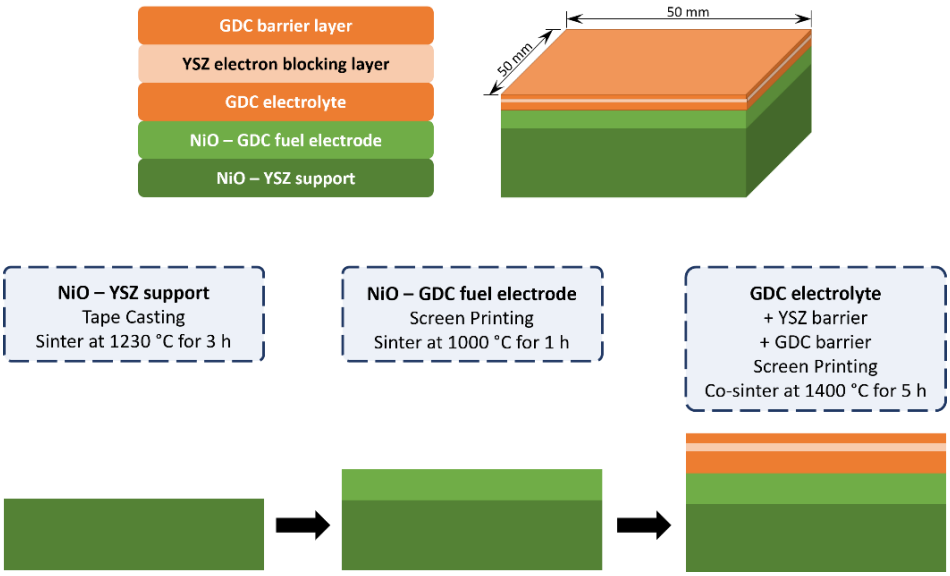

Fig. 1 Complete manufacturing process for the fabrication of half cells, consisting of substrate sintering, fuel electrode printing and pre-sintering and the printing and co-sintering of the 3-layer GDC/YSZ/GDC electrolyte.

3. Results and discussion

The results of the dilatometric measurements are presented in Fig. *2* as the shrinkage rates of the different powders. As can be seen from the figure, for the GDC powder the temperature of the sintering onset increases with increasing calcination temperature. In contrast, the maximum shrinkage rate is reduced with increasing calcination temperature. When compared to the sinter onset of the YSZ, the closest sinter onset is achieved by GDC powder that was pre-calcined at 1340 °C. The maximum shrinkage rate of the YSZ powder occurs at the electrolyte sintering temperature of 1400 °C. However, none of the GDC powder's maximum shrinkage rate temperatures match that. For GDC calcined at 1340 °C this only occurs above 1400 °C while for all the others it's below. The untreated GDC exhibits its highest shrinkage rate at roughly 820 °C. This mismatch in maximum shrinkage rate temperature and sintering temperature could explain the lack of densification. Furthermore, the decline in maximum shrinkage rate is also contributing to the poor densification when compared to the YSZ.
Doping the GDC powder with cobalt ions (GCDC) increased the maximum shrinkage rate to almost 0.4 %/min. The doping also decreased the sinter onset and the maximum shrinkage rate temperature to 950 °C and 1100 °C respectively when comparing it to the same but undoped powder that was pre-calcined at 1230 °C.

The difference in sintering behavior and its effect on microstructure formation is also evident when looking at polished and etched pellet surfaces in Fig. 3. GDC that was pre-calcined at 1230 °C shows significantly smaller grains and higher porosity when compared with both the doped GCDC powder and the YSZ powder. Although the highest shrinkage rate of the GCDC doesn't occur at the sintering temperature of 1400 °C, as for YSZ, they show similar microstructures with large grains and almost no residual porosity. However, the GCDC pellet exhibits a secondary phase along some parts of the grain boundaries and inside of inclusions.

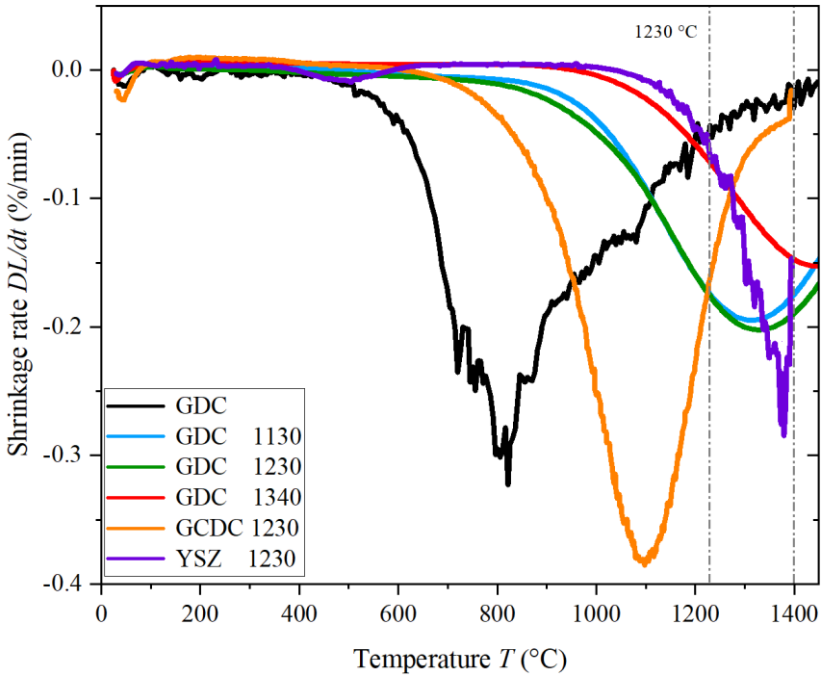

Fig. 2 Temperature vs. shrinkage rates derived from dilatometric measurements. Each measurement was conducted with a continuous heating rate of 3 K/min to 1400 °C which was held for 5 h with subsequent cooling at 5 K/min.

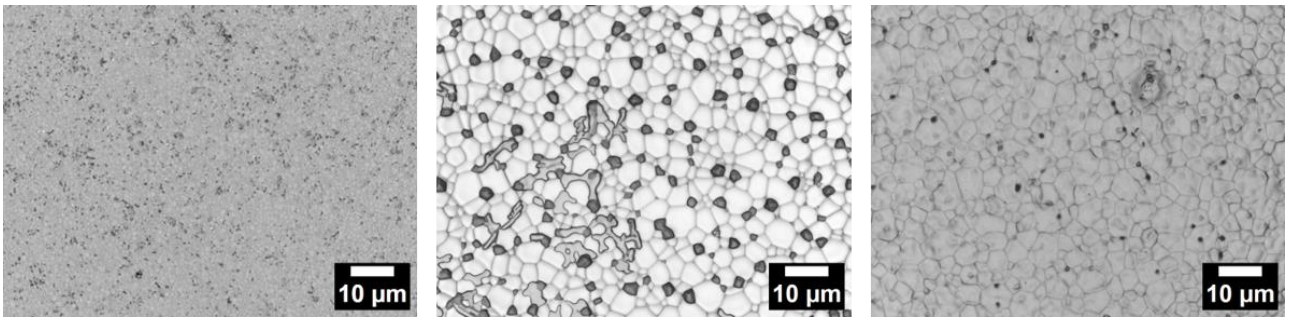

Fig. 3 Laser micrographs of pellets from the dilatometer measurements. Left: GDC calcined at 1230 °C. Middle: GCDC. Right: YSZ calcined at 1230 °C.

When looking at the rheological results, only selected pastes are considered. For example, the behavior of pastes with bimodal powder is almost identical, so that only the viscoelastic behavior of paste B is shown as a representative of pastes A to E and G.

Comparing the results of the oscillatory amplitude sweep test on the left in Fig. 4 indicates, that pastes with a bimodal powder don't exhibit a flow point ($G' = G''$), while pastes with a unimodal powder show the opposite. In the bimodal Paste B, the viscous behavior represented by the loss modulus G'' is always dominant, meaning that there is no transition into flow as the paste is already in a flow state even without the application of load. Therefore, no FTI could be calculated for these pastes. However, pastes made from unimodal powder exhibit the desired viscoelastic properties and a transition from yielding into flow. Here, elastic behavior is dominant until a threshold strain is reached. Only after this point, viscous behavior is more dominant ($G'' > G'$). A reason for the difference in viscoelastic properties between pastes made from bimodal and unimodal powder could be that in pastes with bimodal powders, the internal network that results from the interaction between binder and ceramic particles, gets disturbed by the minor fraction of larger particles or agglomerates. This, in turn, would lead to network instability.

When there is no such obstruction to the network, the binder seems to gain more importance. On the right of Fig. 4, pastes made from the same unimodal powder are compared with the only difference being the polymer chain length of the binder that was used. The higher FTI value for Paste F indicates a more gradual transition into flowing, which is also visible by the size of the yield range. Additionally, the internal network strength of this paste seems to be lower than that of the paste with the longer chained ethyl cellulose. It seems that a longer polymer chain probably leads to more energy being able to be stored inside the network, which is represented by the storage modulus G′. More interestingly however, in Paste E, the viscous and elastic contributions to the behavior are almost equally pronounced. On the other hand, in the paste with 10 cp ethyl cellulose, the elastic behavior is significantly more dominant than the viscous behavior before the flow point is reached. This could also explain why the transition into flow is more abrupt in Paste E.

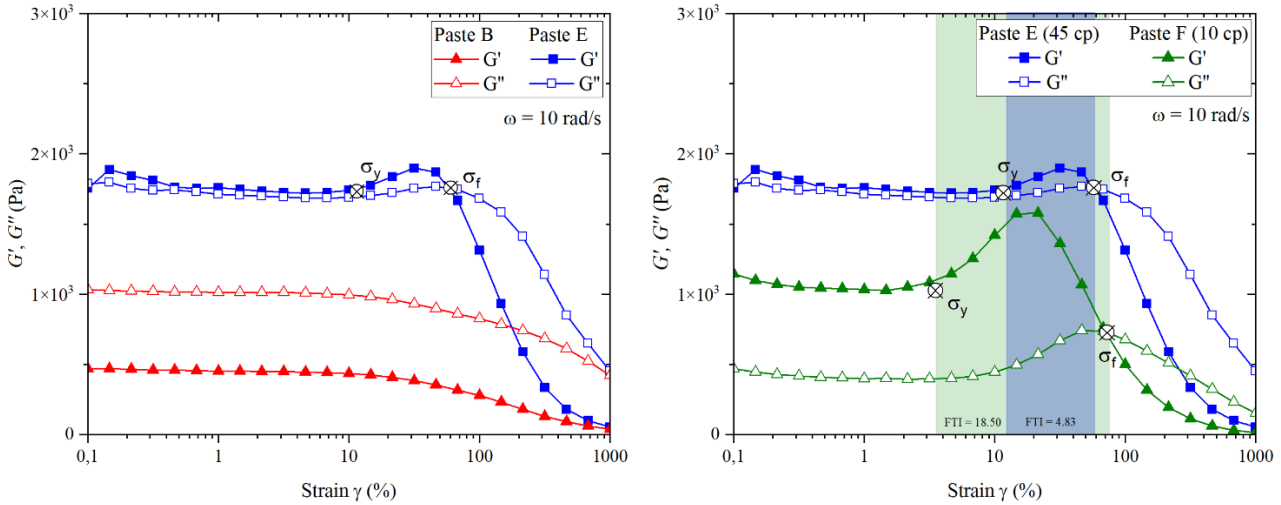

Fig. 4: Strain based oscillatory amplitude sweep test for multiple electrolyte pastes. Left: Comparison of pastes with a bimodal powder (Paste B, red) with pastes made with a unimodal powder (Paste E, blue. Right: Comparison of pastes made with the same unimodal powder but different binder polymer chain lengths (Paste E, 45 cp EC, blue and Paste F, 10 cp EC, green).

The similarity in the viscous and elastic components is also evident when looking at the recovery times of these pastes in Fig. 5. In the first measurement interval, at rest conditions, the same behavior as from the oscillatory amplitude sweep test is seen here for both pastes. Upon destruction of the internal network structure in interval II however, both pastes behave very differently during reconstruction in interval III. While Paste F rebuilds its structure within roughly 10 s ($G' > G''$), for Paste E it takes 385 s. This trend is exactly opposite to the behavior of the transition to flow as described before. Paste E transitions more rapidly or abruptly into flow than Paste F, but rebuilding of the internal structure takes longer. One explanation for that might be the chain length of the polymer component. A shorter chain might be easier or quicker to rebuild into a strong network, than a longer chain. This, however, would not explain the more gradual yielding of a paste with a shorter polymer. Nevertheless, these results provide important insights into the printability of pastes and the resulting print quality, as the fast-recovering Paste F showed severe drying cracks which rendered the cell unusable. Layers printed with the slower recovering Paste E showed smooth surfaces with no cracks or screen imprints, indicating good leveling of the paste.

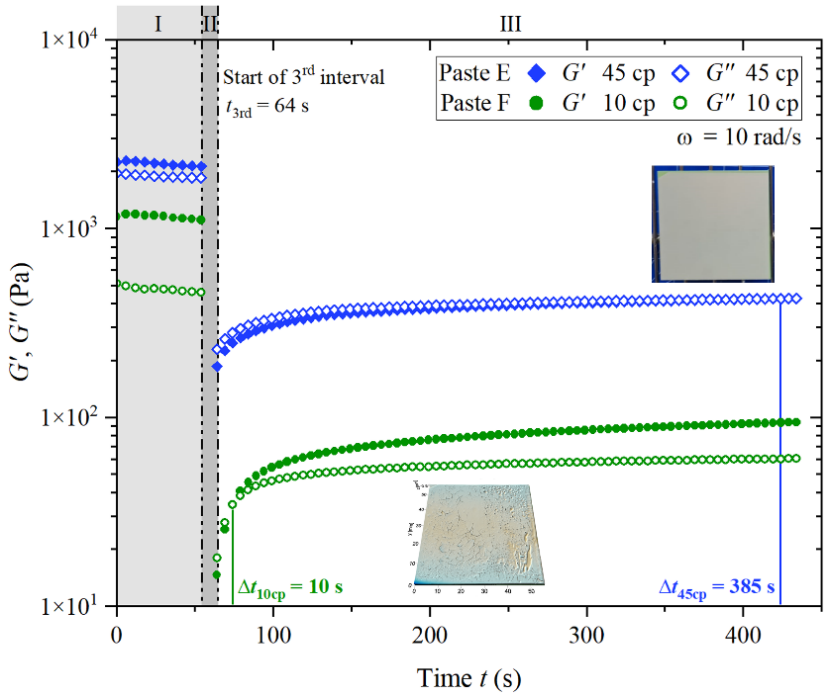

Fig. 5 3ITT results of two electrolyte pastes. Paste F (green, short polymer binder) and Paste E (blue, long polymer binder). For both pastes, recovery times are indicated.

FigureFig. 6 compares selected representative microstructures of polished cross sections. The top row shows half cells with one GDC electrolyte layer. The bottom row shows half cells with a fully built GDC/YSZ/GDC 3-layer electrolyte. All GDC electrolyte layers show residual porosity. The highest porosity can be seen in the electrolyte layer with the bimodal powder pre-calcined at 1340 °C. The high porosity is consistent with the results of the dilatometer measurements, which showed that the sintering activity of this powder is comparatively low and that the maximum shrinkage rate has not yet been reached at the sintering temperature. Higher densities of the GDC layers were achieved with the powders that were pre-sintered at 1230 °C. Although the doped GCDC powder (Paste G) showed a significantly higher maximum shrinkage rate in the dilatometer measurements, no significantly higher densification was observed here compared to the identically produced but undoped powder in layers made with Paste B. This suggests that the sintering behavior of pellets cannot be fully transferred to that of printed layers. Nevertheless, they can provide valuable hints to the behavior.

When looking at the images of cells with 3-layer electrolytes, the porosity at the interface between GDC and YSZ is striking. The occurrence of this porosity is critical as it could not only weaken the mechanical integrity of the composite, but could also result in a reduction in ionic conductivity due to limited conduction paths [11]. Investigations regarding this will be conducted in future works. However, the porosity can be significantly reduced by using unimodal powder, as shown in the bottom right image. The bulk porosity of the GDC layers also appears to be reduced. The reason for this could be that, in principle, agglomerates or bimodal particle size distributions with small fractions of larger particles hinder the compaction of ceramic bodies. However, the improved rheological properties could also contribute to increased compaction. Due to the adapted viscoelastic properties (see Fig. 4), higher green densities could presumably be achieved during screen printing, which would also lead to higher sintering densities after sintering [12]. Investigation of the influence on green density is planned in future studies. The YSZ layer has virtually no residual porosity in both 3-layer electrolytes.

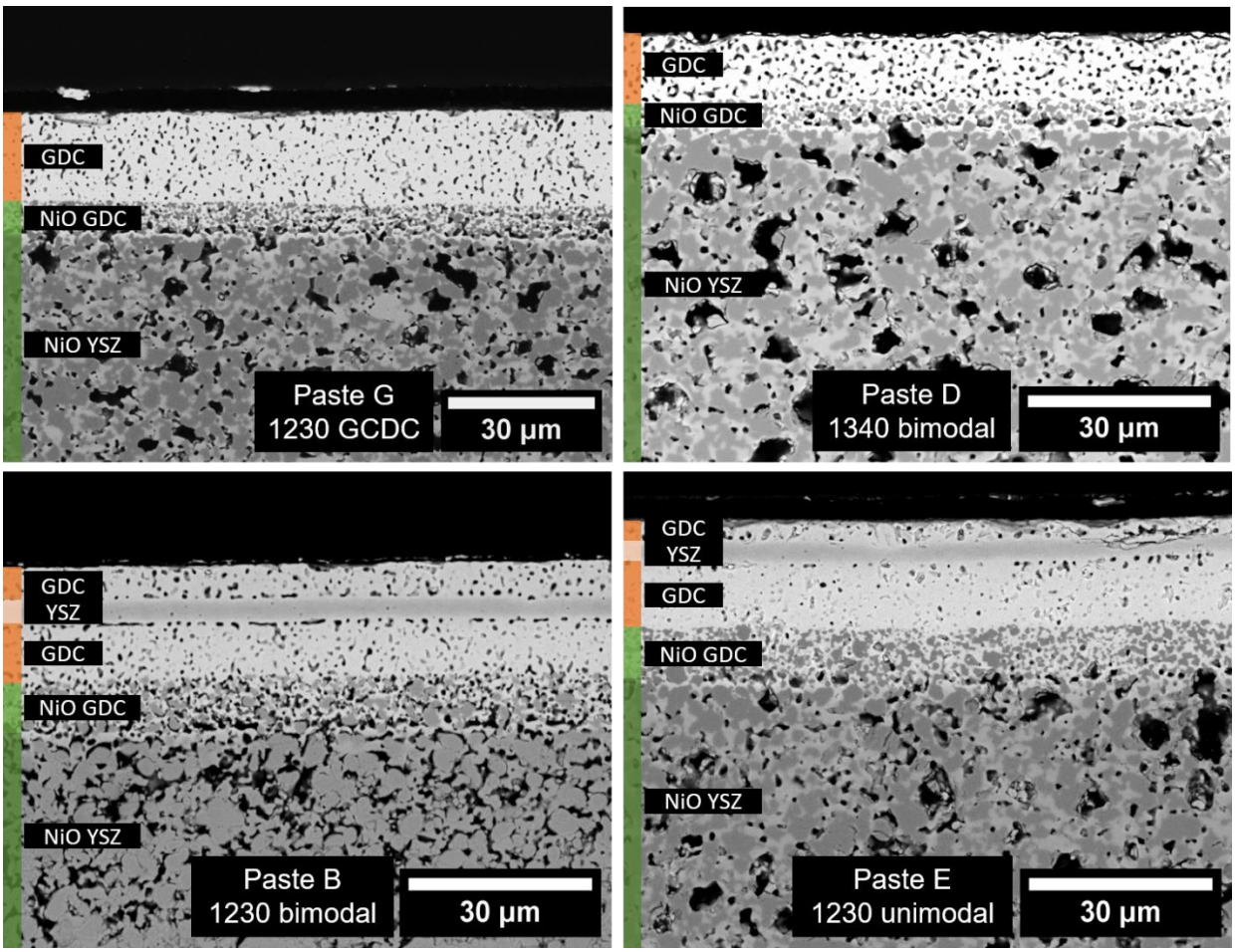

Fig. 6 SEM micrographs of polished cross sections of representative samples. Top row shows samples with only one GDC electrolyte layer. Bottom row shows samples with fully screen-printed GDC/YSZ/GDC electrolytes.

4. Conclusion

Dilatometric measurements of GDC powders revealed significant variations in sintering onset temperatures and maximum shrinkage rates, depending on pre-calcination temperature and doping with cobalt ions. Shrinkage rates decrease with increasing pre-calcination temperature, while sinter onset increases. A mismatch in maximum shrinkage rate temperatures potentially explains observed deficiencies in densification when compared to YSZ. Furthermore, it was proven that doping GDC with cobalt ions can increase the maximum shrinkage rate significantly, resulting in larger grains and no porosity in sintered pellets. However, comparisons between microstructures of pellets and printed layers suggest that sintering behavior may not be directly transferable between these two processing methods.

Additionally, rheological assessments highlight the influence of powder characteristics and binder properties on the viscoelastic behavior of pastes, especially the yielding process and thixotropy. Bimodal powders in the pastes seem to disrupt and weaken the internal paste structure which leads to undesired viscoelastic properties. Furthermore, using unimodal powders in pastes seems to increase the densification of printed GDC layers, while simultaneously decreasing the porosity at the GDC/YSZ interface. The more desirable viscoelastic properties of these pastes probably lead to higher green densities of the deposited layers, which positively influence densification. It was also found that the

employment of short polymer binder chains leads to fast paste recovery times, resulting in the formation of drying cracks and screen imprints.
Overall, investigations into the sintering behavior and rheological properties of GDC powders yield valuable insights into their potential incorporation into solid oxide cells. Future investigations will focus more on elucidating the mechanisms behind the observed phenomena, such as the impact of particle size distribution on compaction and green density. These findings hold promise for enhancing the performance and reliability of solid oxide cells through improved material design and processing control.

Acknowledgments

The authors gratefully acknowledge the funding by the German Federal Ministry of Education and Research. Project: ElChFest (Elektro-chemo-mechanische Modellierung von Ceroxid-basierten Festoxidelektrolysezellen), 03SF0641A.

References

[1] Zhang, J. et al. Boosting intermediate temperature performance of solid oxide fuel cells via a tri-layer ceria–zirconia–ceria electrolyte. J. Am. Ceram. Soc. 106, 93–99 (2023).
[2] Lenser, C. et al. Electro-chemo-mechanical analysis of a solid oxide cell based on doped ceria. J. Power Sources (2022)
[3] Guesnet, L., Bassat, J. M., Grenier, J. C., Chartier, T. & Geffroy, P.-M. Shaping of ceria-based single solid oxide cells combining tape-casting, screen-printing and infiltration. J. Eur. Ceram. Soc. 40, 5662–5669 (2020).
[4] Mücke, R., Menzler, N. H., Buchkremer, H. P. & Stöver, D. Cofiring of Thin Zirconia Films During SOFC Manufacturing. J. Am. Ceram. Soc. 92, S95–S102 (2009).
[5] Inaba, H. Sintering behaviors of ceria and gadolinia-doped ceria. Solid State Ion. 106, 263–268 (1998).
[6] Jud, E., Zhang, Z., Sigle, W. & Gauckler, L. J. Microstructure of cobalt oxide doped sintered ceria solid solutions. J. Electroceramics 16, 191–197 (2006).
[7] Somalu, M. R., Yufit, V., Shapiro, I. P., Xiao, P. & Brandon, N. P. The impact of ink rheology on the properties of screen-printed solid oxide fuel cell anodes. Int. J. Hydrog. Energy 38, 6789–6801 (2013).
[8] Phair, J. W. Rheological Analysis of Concentrated Zirconia Pastes with Ethyl Cellulose for Screen Printing SOFC Electrolyte Films. J. Am. Ceram. Soc. 91, 2130–2137 (2008).
[9] Somalu, M. R., Yufit, V. & Brandon, N. P. The effect of solids loading on the screen-printing and properties of nickel/scandia-stabilized-zirconia anodes for solid oxide fuel cells. Int. J. Hydrog. Energy 38, 9500–9510 (2013).
[10] Wei, P. et al. Go with the flow: Rheological requirements for direct ink write printability. J. Appl. Phys. 134, 100701 (2023).
[11] Schwiers, A., Lenser, C., Guillon, O. & Menzler, N. H. Interdiffusion at electrochemical interfaces between yttria-stabilized zirconia and doped ceria. J. Eur. Ceram. Soc. 43, 6189–6199 (2023).
[12] Mücke, R. et al. High-precision green densities of thick films and their correlation with powder, ink, and film properties. J. Eur. Ceram. Soc. 34, 3897–3916 (2014).

Keywords: EFCF2024, Solid Oxide Technologies, SOE, Rheology, Processing, Screen-Printing